

A numerical study of the impact of climate and emission changes on surface ozone over South China in autumn time in 2000-2050

Q. Liu¹, K.S.Lam^{1*}, F. Jiang², T.J. Wang³, M. Xie³, B.L. Zhuang³, X.Y. Jiang⁴

1, Department of Civil and Environmental Engineering, the Hong Kong Polytechnic University, Hong Kong

2, International Institute for Earth System Science, Nanjing University, Nanjing, China

3, School of Atmospheric Sciences, Nanjing University, Nanjing, China

4, The National Center for Atmospheric Research, Boulder, CO, USA

*Corresponding author Tel: 852 2766 6071; Fax: 852 2334 6389. Email: cekslam@inet.polyu.edu.hk

Abstract

Using the Weather Research and Forecasting Model with Chemistry (WRF/Chem) model, we conducted a series of numerical experiments to investigate the relative contributions of climate and emission change to surface ozone (O_3) over South China for the period of October in 2005-2007 and 2055-57. WRF/Chem was driven by the outputs of Community Climate System Model version 3 (CCSM3). The simulations predict that on average near-surface temperature and water vapor mixing ratio are projected to increase 1.6°C and 1.6 g/kg under A1B scenario. In response to the climate change, the emissions of isoprene and monoterpenes in South China increase by 5 to 55% and 5 to 40%, respectively. The change of climate and biogenic emission can result in a change of -5 to 5 ppb of afternoon surface O_3 mixing ratios, with an average of 1.6 ppb over the land region in South China. Over Pearl River Delta, a region of dense network of cities, the 2000-2050 climate changes increase afternoon mean surface O_3 by 1.5 ppb. The change of anthropogenic emission can result in a change of -3 to 24 ppb of afternoon surface O_3 mixing ratios, with an average of 12.8 ppb over the land region in South China. Our analysis suggests that the anthropogenic emissions have greater impact on the change of surface O_3 concentration over South China compared to climate change. The combined effect of climate and emission can increase afternoon mean surface O_3 over South China by an average of 18.2 ppb in the land region, with the highest increase up to 24 ppb occurring over southeast of Hunan province.

Key words: Ozone; WRF/Chem; Climate change; Biogenic emission; Anthropogenic emission; South China

1. Introduction

Surface ozone (O_3) is formed by photochemical reactions involving carbon monoxide (CO), volatile organic compounds (VOCs) in the presence of nitrogen oxides ($\text{NO}_x \equiv \text{NO} + \text{NO}_2$) under the sunlight. Many studies have pointed out that ground-level O_3 have detrimental effects on human health, plants and ecosystems (Bell M. L., 2005;

Emberson et al., 2003). As a country with rapid urbanization and industrial development in recent years, O₃ pollution is of great concern in China (Chan et al., 2008). Due to the sharp rise in anthropogenic emissions since 1990s, surface O₃ in the background atmosphere of South China has seen its steady increase at an average rate of 0.58 ppbv/yr during the period of 1994-2007 (Wang et al., 2009). As the most urbanized and industrialized regions in South China, Pearl River Delta (PRD) has experienced severe photochemical pollution with surface O₃ levels frequently exceeding the Hong Kong health standard (1-hr average 240 µg/m³ or 120 ppb), especially in autumn season with northerly winds and clear sky conditions (Huang et al, 2005).

In order to protect public health, China air quality managers have implemented a variety of policies to reduce emissions and ambient concentrations of O₃ precursors. However, other than precursor emissions, meteorological factors such as temperature, water vapor, precipitation, cloud cover, wind speed, and mixing depth also play significant roles on O₃ formation and depletion in the boundary layer. Climate change induced by greenhouse gases could significantly affect the meteorological conditions in the future. Thus this potential change should be taken into account when implementing the emission reduction policies aimed at reducing the negative impacts of O₃.

The need for an understanding on the impact of climate change on O₃ formation and depletion using coupled general circulation model (GCM) and chemical transport model (CTM) is highlighted in a number of reviews and recent studies. Jacob et al. (2009) reviewed a large number of GCM–CTM studies. They examined the impact of climate change on O₃ concentrations in regional scales and pointed out that surface O₃ would be projected to increase by 1–10 ppb in summertime at polluted regions. Using global climate and chemistry models, Wu et al. (2008) estimated the future changes in surface O₃ concentrations as a result of future climate and anthropogenic emission changes. Jiang et al. (2008) evaluated the impacts of climate and land use change on

surface O₃ in Houston through a modeling system of a global climate model and Weather Research and Forecast model coupled with Chemistry (WRF/Chem).

Most of the studies investigating the impact in eastern Asia and South China are included in global GCM-CTM study results. Regional model studies have been limited. The aim of this paper is to study the contributions of future climate change and emission change to surface O₃ in South China using WRF/Chem model system. In this paper, South China refers to the area including the provinces of Guangdong, Hainan, Fujian, parts of Fujian, Hunan, Guangxi, and 2 special administrative regions (SAR): Hong Kong and Macau. In section 2, we describe the methodology and the input data adopted in this study. The model performance is evaluated in section 3. In section 4, future climate change and its impact to biogenic emission and surface O₃ are presented. In section 5, the effect of anthropogenic emission change and the combined climate change and emission change effect on O₃ formation are investigated. In section 6, sensitivities of surface O₃ over rural, urban and ocean regions are discussed. We present conclusions and future research suggestions in section 7.

2. Methodology

2.1. Model description and configuration

The WRF/Chem version 3.0 was applied to simulate the O₃ air quality in this study. Detailed descriptions of WRF/Chem model can be found in Grell et al. (2005). Briefly, this is a new generation of regional air quality modeling system developed at National Center for Atmospheric Research (NCAR). The coupled modeling system is composed of meteorological component (WRF) and air quality component (Chem), which are fully coupled using the same coordinates and physical parameterization. Study conducted by Jiang et al. (2010) has shown that WRF/Chem has relatively good capability on simulating trace gases in China.

The detailed options of physical and chemical parameterization scheme used in this

study are shown in Table 1. An Urban Canopy Model (UCM) coupled with the Noah Land Surface Model (Noah/LSM) was adopted for better simulating the urban effect on meteorological conditions and surface O₃ distribution. In the WRF/Chem model, the default U.S. Geological Survey (USGS)-based land cover data is too old to reflect the intensive land-cover change undergoing in China since 1990s. So we mapped the urban land cover data acquired from the 2000 MODIS land cover product into the simulation domains to replace the default USGS data as described by Jiang et al. (2010). For the gas phase chemistry, Carbon-Bond Mechanism version Z (CBMZ) was applied which contains 55 prognostic species and 134 reactions (Zaveri et al., 1999). Based on original Carbon Bond Mechanism (CBM-IV), CBMZ includes reactive long-lived species, revised isoprene chemistry, and optional DMS chemistry. The Model for Simulating Aerosol Interactions and Chemistry (MOSAIC) was adopted as the aerosol chemistry option in simulation, with aerosol size distribution divided into eight discrete size bins (Zaveri et al., 2008). Initial and boundary conditions for the gas phase variables are using the default profiles in WRF/Chem collected from the aircraft measurements over the eastern Pacific Ocean (McKeen et al., 2002). Boundary conditions for O₃ NO_x and CO are varying with altitude. Specifically, at surface, O₃ condition is fixed at 30 ppb, and increasing exponentially to 40 ppbv at 2 km, then increasing to 150 ppb at the model top. There are no adjustments for chemical boundary conditions in the future year simulations which may result in some uncertainty in the model results.

Two nested domains were defined in the simulation, which are shown in Figure 1. The outermost domain (D1) covers the most part of China region and the Korean Peninsula (5–45° N, 90–135° E), with the center point at 27.6° N, 113.1° E, horizontal grids of 100 × 100, and grid spacing of 45 km. The nested domain (D2) covers the southern part of China (15° N–28° N, 108° E–119° E), with 82 × 79 horizontal grids at 15 km grid spacing. From the ground level to the top pressure of 50 hPa, there are 28 vertical sigma layers to all grid meshes, with about 10 layers below 2.0 km above ground level (AGL).

The NCAR Community Climate System Model version 3 (CCSM3) outputs with horizontal resolution T85 ($\sim 1.41^\circ$) are used to drive WRF/Chem model as in Jiang et al. (2008). Outputs from CCSM3 have been adopted by the IPCC Fourth Assessment Report for evaluation (Meehl et al., 2005). The simulation during 2000-2099 is performed with greenhouse gas concentrations followed the A1B scenario from IPCC Special Report on Emission Scenarios (SRES). The A1B scenario is representing a mid-line scenario for carbon dioxide emissions and economic growth compared with other SRES emission scenarios. We choose two periods of three years in 2000s (2005-2007) and 2050s (2055-2057) to provide the regional model with present and future years meteorological inputs.

2.2. Emission inventory

The anthropogenic emissions for the present year 2000s are obtained from the 2006 Intercontinental Chemical Transport Experiment-Phase B (INTEX-B) inventory (Zhang et al., 2009). It is a new emission inventory for Asia with $0.5^\circ \times 0.5^\circ$ horizontal resolution developed to support INTEX-B field campaign. The emissions include sulfur dioxide (SO_2), NO_x , CO, VOCs, PM10, PM2.5, black carbon (BC) and organic carbon (OC) from power, industry, residential, and transportation sectors. Offshore shipping Emissions are not included in this inventory. The Transport and Chemical Evolution over the Pacific (TRACE-P) biomass burning emission for the year 2000 has been applied to estimate the Asia biomass burning (Streets et al., 2003). We then specified monthly variations of anthropogenic and biomass burning emissions following the work of Zhang et al. (2009) and Streets et al. (2003), respectively. Figure 2a shows the distributions of monthly averaged NO emissions from the major anthropogenic sources and biomass burning as well for the inner domain. Strong NO emissions ($>50 \text{ mol km}^{-1} \text{ hr}^{-1}$) were found mainly over PRD, east of Guangdong province, and coastal region of Fujian province. We estimate the future year anthropogenic emissions by multiplying the 2006 base year emission inventory with the regional growth factors for the Special Report on Emissions Scenarios (SRES)

A1B scenario. The growth factors in China and Southeast Asia are 1.82, 2.11, and 2.84, for CO, NO_x, and NMVOC respectively, which are calculated following Wigley et al. (2002).

Biogenic emissions of O₃ precursors are computed locally using the Model of Emissions of Gases and Aerosols from Nature (MEGAN v2.04) model coupled within the WRF/Chem model (Guenther et al., 2006). Emission rates of biogenic compounds are calculated on the basis of vegetation and meteorological parameters. Under standard conditions, as shown in Figure 2b, high isoprene emission rates are found in the forested regions mainly over Fujian, Hunan, and southern part of Hainan province, while the emission rates in most Guangxi, Guangdong province are relatively low. Meteorological datasets comprising 2-m temperature, surface pressure, and downward solar radiation are provided from WRF model. Climatological surface air temperature and downward solar radiation datasets are provided by CCSM monthly-mean output data of current (2005–2007) and future (2055–2057) years. Since the biogenic emissions are estimated based on the simulated meteorological parameters, they are allowed to change in response to climate change. Totally, hourly emissions of 138 compounds were estimated by Megan model which are grouped into 20 classes. It should be noted that in this study the changes in NO_x from lightning and stratosphere-troposphere exchange (STE) of O₃ are not accounted in the model.

2.3. Experiments design

This study conducts five cases of numerical experiments to evaluate the climate change impact, the anthropogenic emission change impact and their combined impacts on surface O₃ concentration. Different sets of simulation periods, meteorological conditions, and anthropogenic emissions are listed in Table 2. The control experiment CL2000EM2000 was driven by the meteorological conditions of year 2000s and the INTEX-B anthropogenic emission at 2006 with biomass burning emission obtained from TRACE-P. CL2050EM2000 was driven by the anthropogenic

emissions of 2000s but with the meteorological conditions of 2050s. CL2000EM2050, CL2050EM2050 were carried out with 2050s anthropogenic emissions, but with 2000s and 2050s meteorological conditions, respectively.

Methane is a long lifetime species, which is not dynamically simulated in WRF/Chem model. Also, it is not regulated in local scales. So CH₄ concentration was not increased when conducting the "emission change" scenarios (CL2000EM2050, CL2050EM2050). However, on a global scale, CH₄ plays an important role in determining background O₃ concentrations. We add a sensitivity experiment METH2050 to evaluate the impact of CH₄ emission change on surface O₃. The CH₄ mixing ratio was increased to 2.90 ppm at 2056 under the A1B scenario.

Due to the limitation of computing resources, each case was run for three consecutive October (2005–2007 or 2055–2057) to represent the autumn conditions of present and future climate, since the seasonal O₃ pattern for the period 1994–2007 shows a clear autumn maximum with peaks in October (Wang et al., 2009). Each simulation starts at 0000 UST 29 September. With the initial 41 hours of the model spin-up time, simulation results of the whole October were analyzed.

3. Evaluation of model performance

In our study, the meteorological initial and boundary conditions of WRF/Chem are provided by a global climate model instead of reanalysis data. In order to evaluate the model performance and downscaling effect, simulation results of meteorological factors are compared with the global GCM outputs, since the CCSM3 outputs used for the comparisons have been extensively evaluated (Collins et al., 2006).

Using sensitivity analysis (MM5-CMAQ), Wei (2012) showed that the peak O₃ concentrations would increase from 270 ppb to 301 ppb due to the rise of air temperature under a tropical cyclone scenario in PRD region. Owing to the

importance of temperature on photochemical reaction and biogenic emission, the following evaluation mainly focuses on 2-m temperature (hereafter called surface temperature). Figure 3 shows that the large-scale spatial patterns of monthly mean surface temperature over East Asia simulated by CCSM and WRF/Chem are similar, which implies that WRF/Chem performed relatively well in the simulation of surface temperature. Also, both models show the surface temperature decreased gradually from the southeast ocean regions to the northwest China.

Daily mean surface temperature observed at 47 meteorological stations over South China provided by the National Climatic Data Center (NCDC) (black dots in Figure 1b) were compared with simulations in October during 2005-2007. Overall, the simulated surface temperature was slightly lower than the observed data, with mean bias of -0.63°C . The respective correlation coefficient is 0.91, reflecting good agreements between the observation data and simulation results. However, there are large biases reaching as high as 1 to 2°C at the sites Jian and Ganzhou in Jiangxi province, which subsequently may result in some biases in surface O_3 concentration (Figure 4).

The diurnal cycles of monthly averaged surface O_3 concentrations at 11 major sites over Hong Kong area were also evaluated. These sites are maintained by Hong Kong Environment Protection Department. The locations and the characteristics of each site can be found at <http://www.epd-asg.gov.hk/english/backgd/quality.html>. The result shows that the simulation well captured the diurnal cycles of surface O_3 concentrations (Figure 5). On average, during daytime, the simulated O_3 concentration was slightly higher than the observed data. However, the model underestimates the O_3 concentrations at night. The underestimation of O_3 concentrations during the nighttime was probably due to the inaccuracies in nighttime O_3 precursor simulations and physical processes as well. It is interesting to note that the simulated concentrations of total oxidant O_x (O_3+NO_2) agree well with the observation results while at the same time NO_2 was overestimated but O_3

underestimated. It is possible that titration of O₃ by NO is more efficient in model than observations or higher modeled PBL height could lead to the underestimation of O₃ concentrations during the nighttime. Furthermore, the monthly average O₃ concentrations at 10 sites operated by Guangdong Province Environmental Monitoring Center over PRD region (Figure 1c) were also evaluated. The result indicated that the model has a relatively good performance in simulating surface O₃ over PRD region, with mean bias at -0.9 ppb (Table 3). We also notice that the model also well captured the high O₃ at TH and XP sites.

4 Climate change and its impact on ozone air quality

4.1 Regional climate change

Since the meteorological factors in the planetary boundary layer have significant effects on the photochemical processes, it is necessary to analyze the changes of the meteorological factors over the period between the 2000s and the 2050s. The differences of meteorological variables including 2-m temperature, 2-m water vapor mixing ratio, PBL height, and 10-m wind speed were calculated based on the simulations CL2050EM2000 and CL2000EM2000 for the inner domain.

Figure 6a depicts the change of 2-meter temperature during 12–18 LST simulated by the regional model for October in 50 years time. Owing to the increase of green house gases, average afternoon surface temperature is predicted to increase by 1.6 °C over the entire inner domain. The highest increases of 2 to 2.8 °C occurs over the northeast and northwest area of the modeling domain, while surface temperature increases are smaller over southwest part of Guangdong province, Hainan, Guangxi and the ocean. Figure 6b shows that there is a significant increase of 2-m water vapor mixing ratio occurring over southern China, with the highest increase up to 2.0 g/kg over Taiwan Strait. Average near surface water vapor is predicted to increase by 1.6 g/kg over the entire inner domain. In response to the significant surface warming, evaporation from the ocean will increase. Higher temperature in the future allows the atmosphere to

hold more water. Figure 6b also shows that the change of 2-m water vapor over Ocean is much larger than over land. The pattern of changes in PBL height is quite similar to the spatial distribution of temperature change. The largest warming occurs over northeast and northwest area of the modeling domain results in enhanced mixing in these areas where the PBL height could increase up to 80m. The largest decrease up to 120 m in PBL height occur over areas including the Leizhou Peninsula, the eastern seaboard of Guangxi and the southeast portion of modeling domain (Figure 6c). A day time reduction of near-surface wind speed is predicted over Jiangxi, Fujian, Hainan and part of Guangdong, Hunan (Figure 6d).

4.2. Changes in Surface Biogenic Emissions driven by climate change

For their contributions to the formation of surface O₃, the study of estimating biogenic emissions is of great concern at both regional and local scales. Meteorological conditions that have been known to be associated with high biogenic emissions are high radiation, high temperatures, and high relative humidity.

Our model simulates a significant increase of isoprene and monoterpenes emissions from 2000s to 2050s in response to the change of radiation and surface temperature. Figure 7b shows the isoprene emissions increased by 5 to 55% in October from 2000s to 2050s. The highest percentage up to 45 to 55% occurs over the northwest and northeast area of the modeling domain. Figure 7d shows monoterpenes also increase considerably by 5 to 40%. The predicted percentage increases in isoprene and monoterpene emissions are consistent with the results reported by Zhang et al. (2008). They examined the sensitivity of BVOC emissions to warmer climate in future in the United States under the A1B scenario and found that the isoprene and terpene emissions are projected to increase 20–92% and 20–56% respectively by 2050s. The significant increase is largely determined by the large temperature increase and high forest coverage over this region. According to Lerdau et al. (1997) experiments, the emission rate may increase rapidly with increasing surface temperature from 15°C to

40°C. Although above 40°C, high temperature can inhibit the biogenic emission production. However there is no predicted hourly surface temperature higher than 40°C during the simulation period in this study.

On an absolute change basis, the highest increase in isoprene emissions occurs over the northeast area of the modeling domain (Jiangxi and Fujian mountain area), with an increase up to 6.5 mol km⁻² hr⁻² (Figure 7a). On average, the isoprene emissions are predicted to increase by about 1.0 mol km⁻² hr⁻². The changes of monoterpenes emissions follow a pattern similar to isoprene, with the highest increase up to 2.0 mol km⁻² hr⁻² occurring over the Jiangxi, and Fujian mountain area (Figure 7c).

4.3. Changes in Surface O₃ driven by climate change

Our model simulates a significant difference of the O₃ concentrations between the CL2050EM2000 and CL2000EM2000 within the period 12–18 LST (Figure 8a). In CL2050EM2000, the anthropogenic emissions at 2050s follow the same inventory at 2000s. In response to the change of meteorological variables, autumn-time afternoon O₃ concentrations change vary from -5 to 5 ppb across the inner domain. Over most parts of the land region, the surface O₃ concentration is predicted to increase by 1 to 5 ppb. Over the land region, the average surface O₃ concentration is predicted to increase 1.6 ppb. The regions with large increases are close to the regions with significant increase of temperature and biogenic emissions, such as the south of Jiangxi, Hunan, west of Fujian, and north of Guangdong province. The area of east Hunan and most parts of Jiangxi has the greatest magnitude of increase with concentrations increase between 3 and 5 ppb. The increases in afternoon O₃ concentrations are consistent with the 1 to 8 ppb increase over the Houston area estimated by Jiang et al. (2008) using a similar model system during the summertime by 2050s. On the other hand, the largest decrease of about 4-5 ppb is found over South China Sea. Using the coupled MM5 and CMAQ model, Nolte et al. (2008) have shown that O₃ over the Pacific Ocean decrease by 1 to 3 ppb for the

September/October period based on the A1B scenario due to increasing humidity.

The change of meteorological conditions for future climate scenario can alter the concentrations of O₃ and its precursors NO_x and VOCs through the impact on emission, chemical reactions, transport and deposition processes. Future climate changes in temperature and radiation increase the biogenic isoprene emissions up to 55% compared to present-day simulation. Thus, the isoprene mixing ratios is predicted to increase 30 to 80 ppt over the rural forest regions (Figure 8c). NO_x emissions from soil increase in the 2050 climate due to higher soil temperature and moisture. The thermal decomposition rate for peroxyacetyl nitrate (PAN) is highly dependent on temperature (Sillman et al., 1995). Since the increasing temperature in the 2050s can enhance the decomposition rate of PAN (Figure 8d), there will be more NO_x and HO_x radicals reproduced to facilitate the O₃ formation (Steiner et al., 2006). Meanwhile, the decreased wind speeds near the emission source regions, over Jiangxi, Fujian, Hainan and part of Guangdong, Hunan province, are favorable for the accumulation of the O₃ precursor. Additionally, in response to elevated atmospheric moisture in the future, the reaction between water vapor and O(1D) produces more HO_x radicals into the photochemical cycle. Over clean ocean regions with low NO_x emissions, this reaction results in the destruction of O₃ production and therefore lowering surface O₃ concentration. On the contrary, near high anthropogenic emission regions where NO_x is in abundant supply, HO₂ reacts with NO injecting additional NO₂ to the NO-NO₂-O₃ system and resulting in additional production of O₃. At the same time, due to the increase of OH radicals, the reaction between NO₂ and OH creates more nitric acid over high anthropogenic emission regions (Figure 8b).

The boundary layer O₃ budget was calculated to explore the changes in physical and chemical processes in O₃ formation between CL2000EM2000 and CL2050EM2000. Fig. 9 shows the results of three main processes over the inner domain: O₃ gas phase chemical production (CHEM); O₃ horizontal transport (TRAN); and O₃ deposition (DEP). In response to the climate change and the subsequent increase in biogenic

emission, CHEM process changes vary from -5 to 6 ppb/hr in the afternoon time. The increases of O₃ production in boundary layer over 3 ppb/hr induced by gas phase chemical reaction are found in PRD region and the southeast part of Hunan province. The maximum increases of CHEM process located in the area with great increase of temperature and also high anthropogenic and biogenic emissions. Over the South China Sea with low NO_x emissions, the increase of water vapor would result in a -1 to -5 ppb/hr in CHEM process (Figure 9a). The changes in TRAN process are closely related to the variation of horizontal wind speed, wind direction. TRAN process increases 0 to 4 ppb/hr over most part of the inner domain. The PRD region and southeast part of Guangdong with high anthropogenic NO_x emission have the largest decrease in O₃ transport, ranging from -1 to -7 ppb/hr (Figure 9b). Figure 9c shows that the change in DEP process is between -2 to +2 ppb, basically there is little change in deposition process. Although the surface O₃ will increase in future, at the same time convection will also be enhanced due to warmer temperature. Increase in downward flux due to diffusion will be offset by increase in upward flux due to increase in convection activities. It can be seen that the changes in boundary layer O₃ budget was dominated by the CHEM process. The TRAN and DEP processes were relatively small compared to the CHEM process except in PRD region.

5. Impact of anthropogenic emission change on ozone air quality

According to IPCC SRES report, anthropogenic emissions of O₃ precursors including NO_x, CO, and VOC are projected to increase by 82%, 111%, and 184% compared to the 2000s emission level under A1B scenario in developing countries. The changes in surface O₃ due to emission change are calculated on the basis of two simulations: CL2000EM2050 and CL2000EM2050.

Figure 10a displays the difference in simulated O₃ mixing ratios between CL2000EM2050 and CL2000EM2000. The change of anthropogenic emission can

result in a change of -3 to 24 ppb of afternoon surface O₃ mixing ratios, with an average of 12.8 ppb over the land region in South China. The highest increases of 15 to 24 ppb occurs over west Guangdong and most parts of Guangxi province, whereas an obvious decrease about 0 to 3 ppb is found over the PRD region. There is a significant increase of surface O₃ over most of South China except PRD region. The PRD region is located in the central southern coastal part of Guangdong province including three metropolitan cities of Guangzhou, Shenzhen, Hong Kong and other seven medium and small cities. Substantial economic development leads to high air pollutant emissions in this region. Owing to the significant increase in NO_x mixing ratio at 2050s level, O₃ concentrations are depressed through titration effect ($O_3 + NO = NO_2 + O_2$).

Figure 10b illustrates an increase in surface O₃ in the regions due to the combined effect of climate and emission changes. There is a significant increase of surface O₃ over the whole inner domain with the highest increase of 24 ppb occurring over southeast of Hunan province. On average the surface O₃ is predicted to increase by 18.2 ppb over the land region. Compared to the single anthropogenic emission effect, the combination would induce a greater increase of O₃ over land region. However, in the clean ocean area, the destruction of O₃ production due to the increase of water vapor would result in much lower enhancement.

The emission increase in CH₄ is not considered when conducting the "emission change" scenario (CL2000EM2050, CL2050EM2050). That is CH₄ concentration is kept at 170ppm in both cases. In order to examine the impact on surface O₃ due to increase in CH₄ emission, we calculated the difference between the METH2050 and CL2050EM2050 at the year 2056. Changes in autumn-time afternoon mean O₃ concentrations range from 2.5 to 6.5 ppb (Figure 10c). The largest increases up to 6.5 ppb are found over the regions located to the west part of PRD. On average, the increase of CH₄ induces an increase of 4.2 ppb in O₃ over the entire inner domain.

6. Sensitivity of surface O₃ over Rural, Urban and Ocean regions

The study presented in the above subsections focused on analyzing the effects of climate and emission change on autumn time O₃ concentrations over the whole inner domain. Through the analysis we found that the impacts on surface O₃ concentration vary considerably across the inner domain. It is useful to compare the effects of climate and emission change over different landscapes. Therefore, three regions of the inner domain were selected to represent rural area, as indicated by box A, urban area, as indicated by box B (PRD), and clean ocean area, as indicated by box C (Figure 1b).

Figure 11 illustrates the spatially averaged contributions of climate change and emission change to afternoon surface O₃ for zones A, B and C. It can be seen that the effect of climate change alone in rural area (zone A) accounts for a larger increase of afternoon O₃ concentrations than in urban area (zone B). The bar chart shows that an increase of 3.9 ppb occurs over the rural area in Jiangxi province due to the effects of climate change. In PRD region, the climate change alone results in an increase of 1.5ppb in afternoon mean surface O₃ concentrations. On the contrary, there is a significant decrease of 4.5 ppb due to the effects of climate change alone in zone C. As we discussed above the significant increase of water vapor induces the destruction of O₃ production over the clean marine area.

Compared to the climate effect, the changes of anthropogenic emission result in a more significant increase of surface O₃ over all three regions. On average, the changes of anthropogenic emission contribute the increase of 11.4ppb, 6.1ppb, 12.1 ppb in zone A, zone B, and zone C, respectively. The combination effects in zone A and zone B have greater influence than the emission change alone, resulting in an increase of 20 ppb and 11.4 ppb on afternoon surface O₃ concentration. The increase of surface O₃ at zone C is much lower with 4.7 ppb.

7. Conclusions

The change of O₃ air quality due to the changes of climate and air pollutant emissions was studied by a series of numerical simulations under different meteorological and emission scenarios using WRF/Chem model. The simulations predict that on average near-surface temperature and water vapor mixing ratio are projected to increase 1.6°C and 1.6 g/kg under A1B scenario. Significant increase of biogenic isoprene and monoterpenes emission in South China due to the climate change can reach 5 to 55% and 5 to 40% respectively. In response to the change in climate and biogenic emissions, the afternoon surface O₃ mixing ratios increase 1.6 ppb over the land region in South China. Over PRD, a region of dense network of cities, the 2000-2050 climate changes increase afternoon mean surface O₃ by 1.5 ppb (zone B). The climate change induces a greater influence over rural area than over the PRD region, with an increase of 3.9 ppb in afternoon surface O₃ concentrations (zone A). 2000-2050 anthropogenic emission changes result in an increase of the surface O₃ afternoon mean by 12.8 ppb on average in the land region. The combination effect of climate and emission change would result in an increase of 18.2 ppb in land region, with the highest increase up to 24 ppb occurring over southeastern part of Hunan province.

This study provides us a scope of understanding how the future climate and emission will affect the surface O₃ air quality over South China. One important conclusion is that even under very stringent pollution control measures so that emission level at 2050s is kept at 2006 level, surface O₃ concentration still increase due to climate change. The second point is that O₃ increase caused by increase in anthropogenic emission (A1B scenario) is much worse than that caused by climate change so emission control measures are mandatory. Third, O₃ control policy is not straight forward. Figure 10a indicates that when anthropogenic emissions are greatly increased, regionally O₃ increased but O₃ over metropolitan area will be reduced due to titration effect.

In this study, we assess the impacts of climate and emission change under the A1B scenario. In order to gain a comprehensive understanding, it is necessary to apply a series of scenarios for investigation in the future. Furthermore, China is undergoing significant urbanization processes and will definitely continue in future decades. The effect of changes in land use should be taken into account.

Acknowledgement

This project was mainly supported by the Hong Kong Research Grants Council (PolyU 5211/09E). This work was partly supported by Project supported by the National Basic Research Program of China (Grant No. 2010CB950704).

Reference

- Barnard, J.C., Chapman, E.G., Fast, J.D., Schmelzer, J.R., Slusser, J.R., Shetter, R. E., 2004. An evaluation of the FAST-J photolysis algorithm for predicting nitrogen dioxide photolysis rates under clear and cloudy sky conditions. *Atmospheric Environment*, 38, 3393-3403,
- Bell, M. L., Dominici, F., Samet, J. M., 2005, A meta-analysis of time-series studies of ozone and mortality with comparison to the National Morbidity, Mortality, and Air Pollution Study, *Epidemiology* 16,436–445.
- Chen, F., Dudhia, J., 2001. Coupling an advanced land-surface/hydrology model with the Penn State/NCAR MM5 modeling system. Part I: model description and implementation. *Monthly Weather Review* 129, 569–585.
- Chan C.K., Yao X.H., 2008. Air Pollution in Mega Cities in China. *Atmospheric Environment* 42, 1-42.
- Chou, M.D., Suarez, M.J., 1994. An efficient thermal infrared radiation parameterization for use in general circulation models. NASA Technical Memorandum, TM-104606, 85 pp.
- Collins, W.D., et al., 2006. The Community Climate System Model Version 3 (CCSM3). *Journal of Climate* 19, 2122–2143
- Emberson, L., Ashmore, M., Murray, F., 2003. *Air Pollution Impacts on Crops and Forests. A Global Assessment* Imperial College Press, London, U.K
- Grell, G.A., Peckham, S.E., Schmitz, R., Mceen, S.A., 2005. Fully coupled “online” chemistry within the WRF model: description and application. *Atmospheric Environment* 39, 6957–6975.
- Guenther, A., Karl, T., Harley, P., Wiedinmyer, C., Palmer, P.I., Geron, C., 2006. Estimates of global terrestrial isoprene emissions using MEGAN (Model of

- Emissions of Gases and Aerosols from Nature). *Atmospheric Chemistry and Physics* 6, 3181–3210.
- Hong, S.Y., Pan, H.L., 1996. Nonlocal boundary layer vertical diffusion in a Medium-Range Forecast model. *Monthly Weather Review* 124, 2322–2339.
- Hong, S.Y., Lim, J.O.J., 2006. The WRF Single-Moment 6-Class Microphysics Scheme (WSM6). *Journal of the Korean Meteorological Society* 42, 129–151.
- Huang, J.P., Fung J.C. H., Lau, A.K.H., Qin, Y, 2005. Numerical simulation and process analysis of typhoon-related ozone episodes in Hong Kong. *Journal of Geophysical Research* 110, D05301.
- Jacob, D.J., Winner, D.A., 2009. Effect of climate change on air quality. *Atmospheric Environment* 42, 51-63.
- Jiang, F., Guo, H., Wang, T.J., Cheng, H.R., Wang, X.M., Simpson, I.J., Ding, A.J., Saunders, S.M., Lam, S.H.M., Blake, D.R., 2010. An ozone episode in the PRD: Field observation and model simulation. *Journal of Geophysical Research* 115, D22305.
- Jiang, X.Y., Wiedinmyer, C., Chen, F., Yang, Z.L., Lo, J.C.F., 2008. Predicted impacts of climate and land use change on surface ozone in the Houston, Texas, area. *Journal of Geophysical Research* 113, D20312.
- Kain, J. S., 2004. The Kain–Fritsch convective parameterization scheme: An update. *Journal of Applied Meteorology* 43, 170–181.
- Lerdau, M., Guenther, A., Monson, R., 1997. Plant production and emission of volatile organic compounds. *Bioscience* 47(6), 373-383.
- McKeen, S. A., Wotawa, G., Parrish, D. D., Holloway, J. S., Buhr, M. P., Hubler, G., Fehsenfeld, F. C., and Meagher, J. F., 2002. Ozone production from Canadian wildfires during June and July of 1995. *Journal of Geophysical Research* 107(D14), 4192.
- Meehl, G.A., Covey C., McAvaney B., Latif M., Stouffer R. J., 2005: Overview of the Coupled Model Intercomparison Project. *Bulletin of the American Meteorological Society* 86, 89–93.
- Mlawer E.J., Taubman S.J., Brown P.D., Iacono M.J., Clough S.A., 1997. Radiative transfer for inhomogeneous atmosphere: RRTM, a validated correlated-k model for the longwave. *Journal of Geophysical Research* 102 (D14), 16663–16682.
- Monin, A. S., Obukhov, A. M., 1954. Basic laws of turbulent mixing in the surface layer of the atmosphere. *Contributions of the Geophysical Institute of the Slovak Academy of Sciences* 151, 163–187.
- Nolte, C.G. Gilliland, A.B., Hogrefe, C., Mickley, L.J., 2008. Linking global to regional models to assess future climate impacts on surface ozone levels in the United States. *Journal of Geophysical Research* 113, D14307.
- Sillman, S., Samson, P.J., 1995. Impact of temperature on oxidant photochemistry in urban, polluted rural and remote environments. *Journal of Geophysical Research* 100,11497-11508.
- Streets D.G., Yarber K.F., Woo J.H., Carmichael G.R., 2003. Biomass burning in Asia: annual and seasonal estimates and atmospheric emissions. *Global Biogeochemical Cycles* 17, 1099.

- Wang, T., Wei, X.L., Ding, A.J., Poon, C.N., Lam, K.S., Li, Y.S., Chan, L.Y., Anson, M., 2009. Increasing surface ozone concentrations in the background atmosphere of Southern China, 1994–2007. *Atmospheric Chemistry and Physics* 9, 6217–6227.
- Wei, X.L., Liu, Q., Lam, K.S., Wang, T.J., 2012. Impact of precursor levels and global warming on peak ozone concentration in the PRD region of China. *Advances in Atmospheric Science* 29(3), 635–645.
- Wigley, T.M.L., Smith, S.J., Prather, M.J., 2002. Radiative forcing due to reactive gas emissions. *Journal of Climate* 15(18), 2690–2696.
- Wild, O., Zhu, X., Prather, M.J., Fast, J., 2000. Accurate simulation of in- and below-cloud photolysis in tropospheric chemical models. *Journal of Atmospheric Chemistry* 37, 245–282.
- Wu, S.L., Mickley, L.J., Leibensperger, E.M., Jacob, D.J., Rind, D., Streets, D.G., 2008. Effects of 2000–2050 global change on ozone air quality in the United States. *Journal of Geophysical Research* 113, D06302.
- Zaveri, R.A., Peters, L.K., 1999. A new lumped structure photochemical mechanism for large-scale applications. *Journal of Geophysical Research* 104, 30387–30415.
- Zaveri, R.A., Easter, R.C., Fast, J.D., Peters, L.K. 2008. Model for simulating aerosol interactions and chemistry (MOSAIC). *Journal Geophysical Research* 113, D13204.
- Zhang, Y., Hu, X.M., Leung, L.R., Gustafson Jr., W.I., 2008. Impacts of regional climate change on biogenic emissions and air quality. *Journal Geophysical Research* 113, D18310.
- Zhang Q., Streets D.G., Carmichael G.R., He K., Huo H., Kannari A., Klimont Z., Park I.S., Reddy S., Fu J.S., Chen D., Duan L., Lei Y., Wang L.T., Yao Z.L., 2009. Asian emissions in 2006 for the NASA INTEX-B mission. *Atmospheric Chemistry and Physics* 9, 5131–5153.

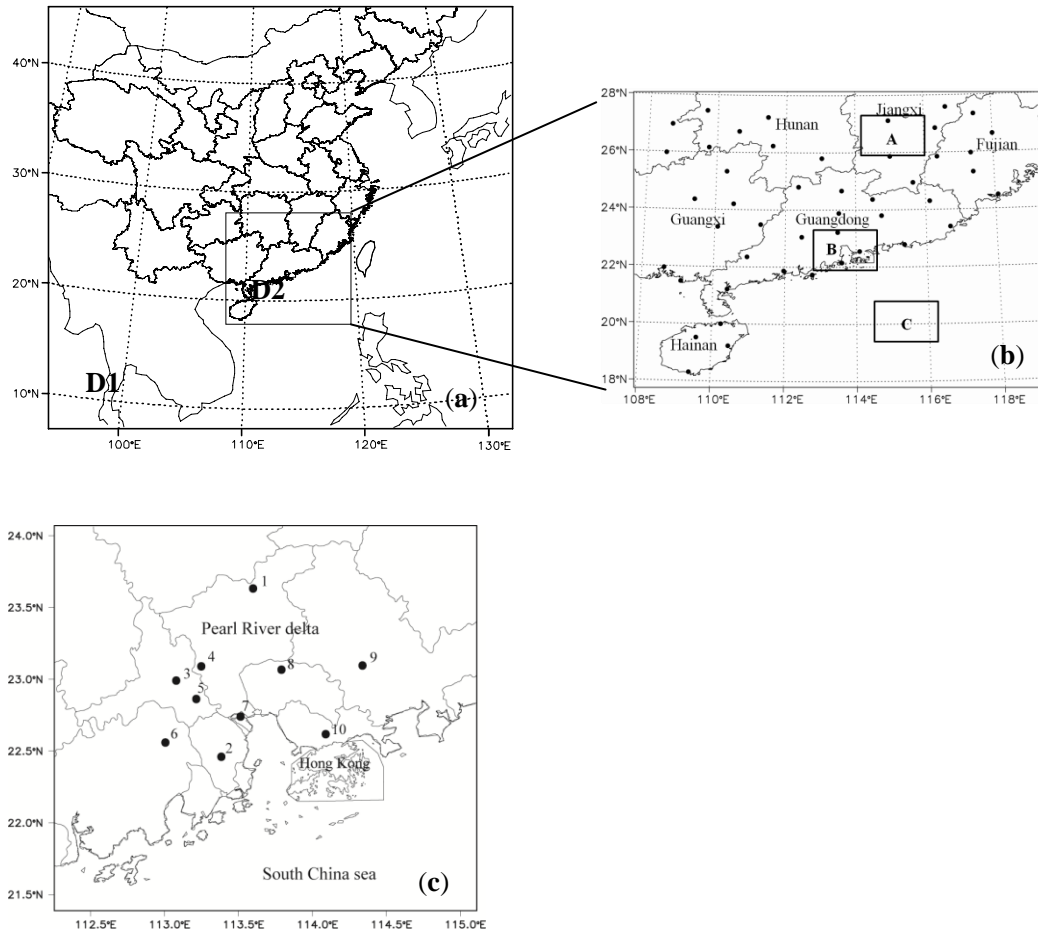


Figure 1. a) Simulation domain setting, b) locations of the meteorological sites for model evaluation (black point) and three selected regions (black square box), c) locations of air quality monitoring sites at PRD region: 1) Tianhu (TH), 2) Zimaling (ZML), 3) Huijingcheng (HJ), 4) Luhu (LH), 5) Shunde (SD), 6) Donghu (DH), 7) Wanqingsha (WQS), 8) Haogang (HG), 9) Xiapu (XP), and 10) Liyuan (LY)

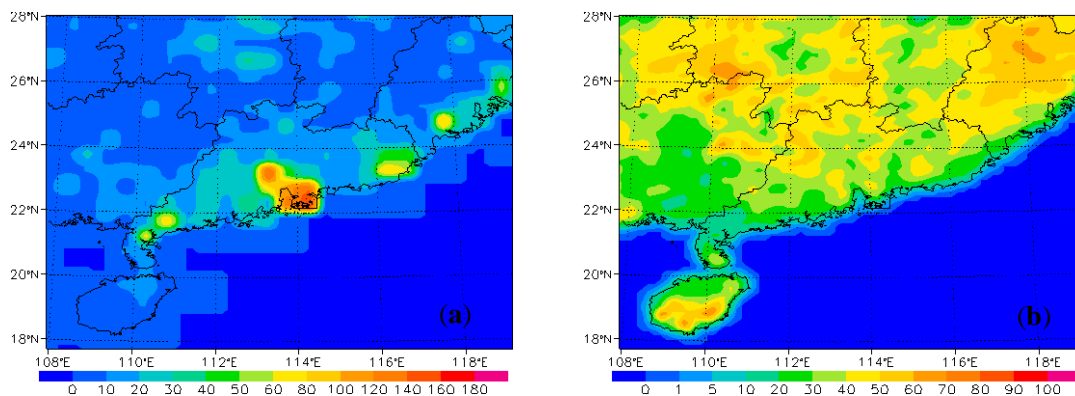


Figure 2. Spatial distributions of (a) daily average anthropogenic and biomass burning NO emissions in October ($\text{mol km}^{-2} \text{hr}^{-1}$) and (b) standard biogenic isoprene emissions generated by MEGANv2.04 ($\text{mol km}^{-2} \text{hr}^{-1}$).

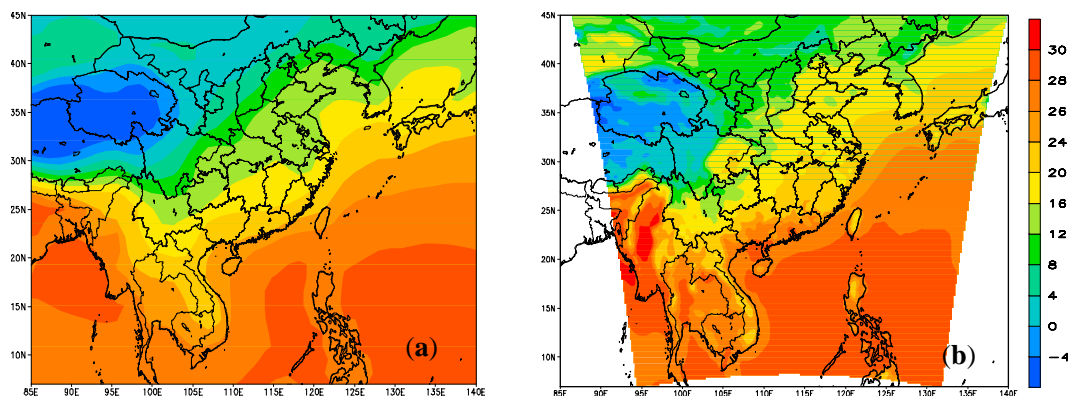


Figure 3 Monthly average surface temperature ($^{\circ}\text{C}$) during October 2005–2007 from a) CCSM outputs and b) WRF/Chem outputs.

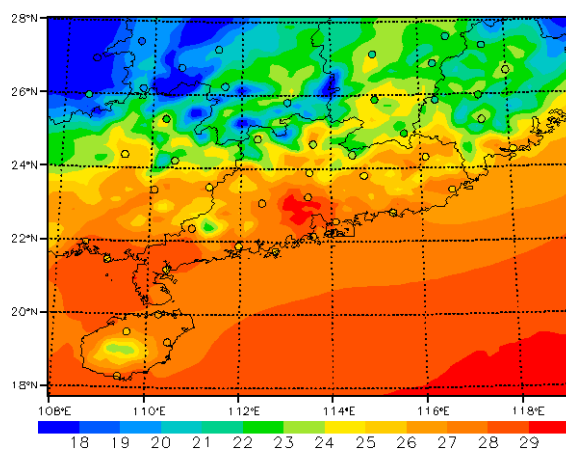


Figure 4 Simulated (shaded) and observed (dot) monthly average surface temperature ($^{\circ}\text{C}$) during October 2005–2007 in South China

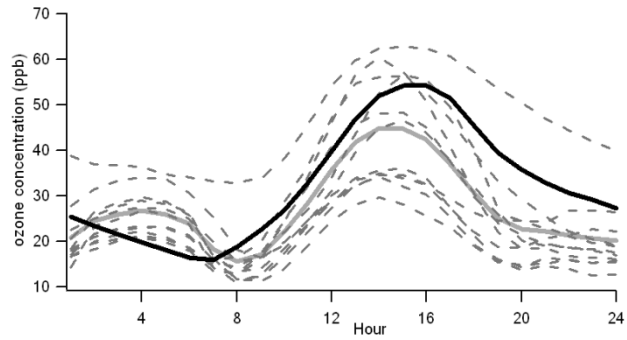


Figure 5. Diurnal cycles of present years O_3 concentrations in October 2005-2007 for observations at 11 stations (dotted lines), mean observed results (gray line) and the mean simulated results (black lines).

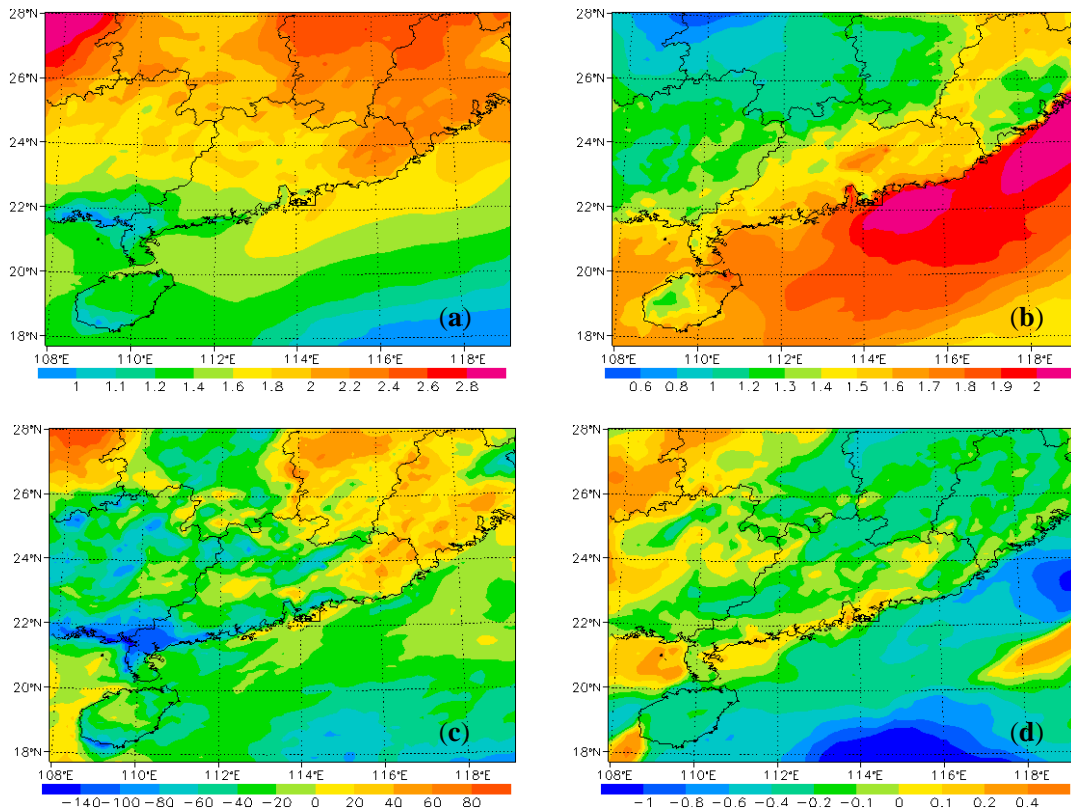


Figure 6. Changes in afternoon average (a) temperature ($^{\circ}C$), (b) 2-m water vapor mixing ratio (g/kg), (c) planetary boundary layer height (m), and (d) 10-m wind speed (m/s) between CL2000EM2000 and CL2050EM2000 simulations for the month of October.

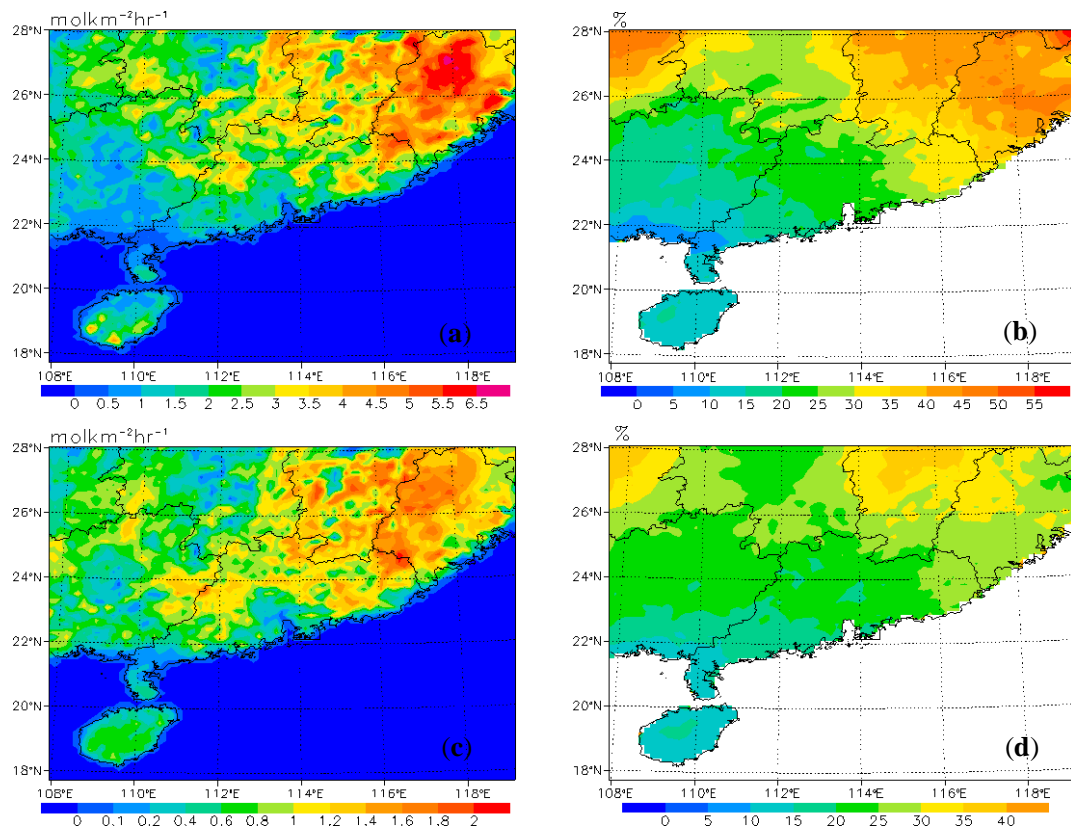


Figure 7. Absolute and percentage changes in emissions of isoprene (a,b) and monoterpenes (c,d) between CL2000EM2000 and CL2050EM2000 simulations for the month of October.

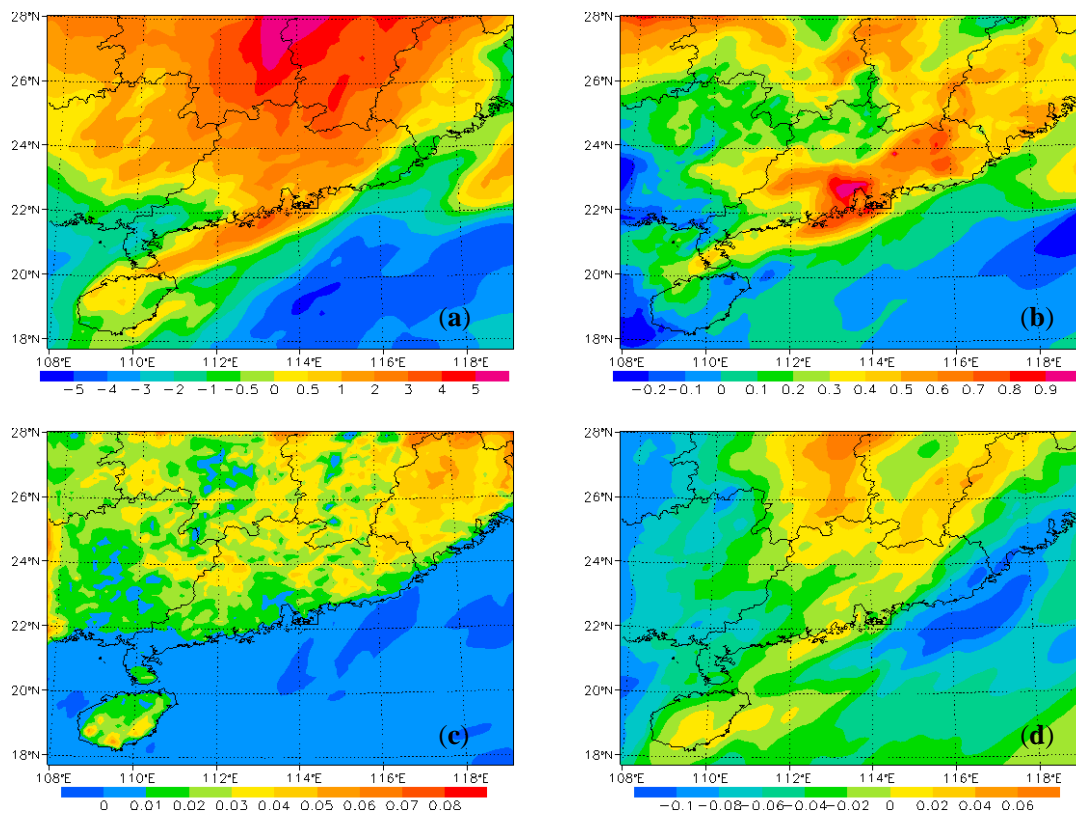


Figure 8. Changes in afternoon average (a) O₃ (ppb), (b) HNO₃ (ppb), (c) Isoprene (ppb), (d) PAN (ppb) between CL2050EM2000 and CL2000EM2000 simulations for the month of October.

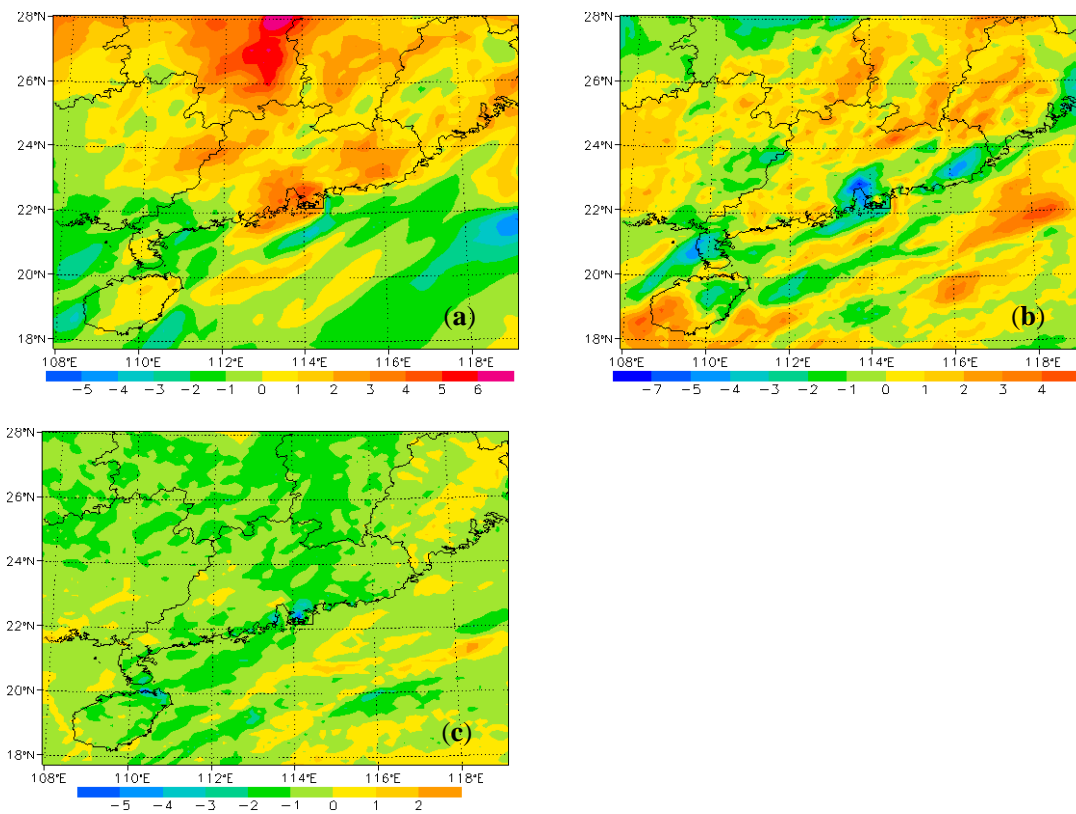


Figure 9. Changes in afternoon average (a) CHEM process (ppb/hr), (b) TRAN process (ppb/hr), (c) Dep process (ppb/hr) between CL2000EM2000 and CL2050EM2000 simulations for the month of October.

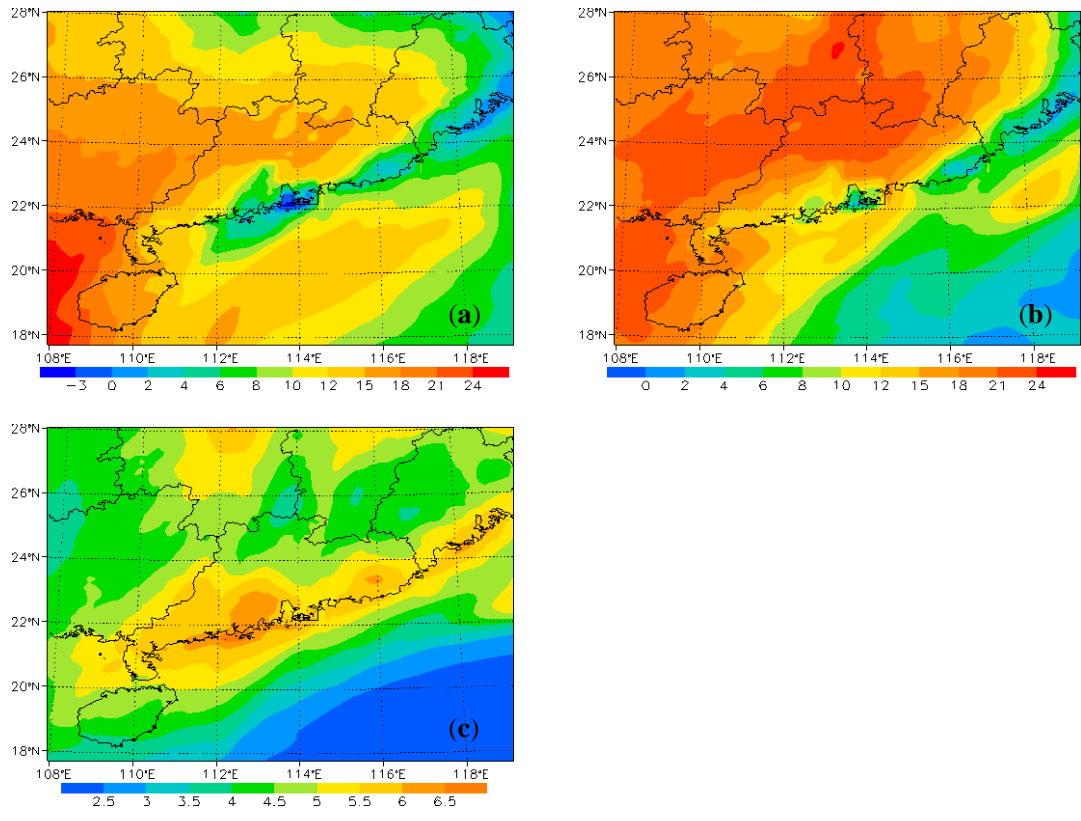


Figure 10. Simulated differences of afternoon average for surface O₃ (ppb) a) between CL2000EM2050 and CL2000EM2000 simulations, b) between CL2050EM2050 and CL2000EM2000 simulations for the month of October, c) between METH2050 and CL2000EM2000 for the month of October at the year 2056

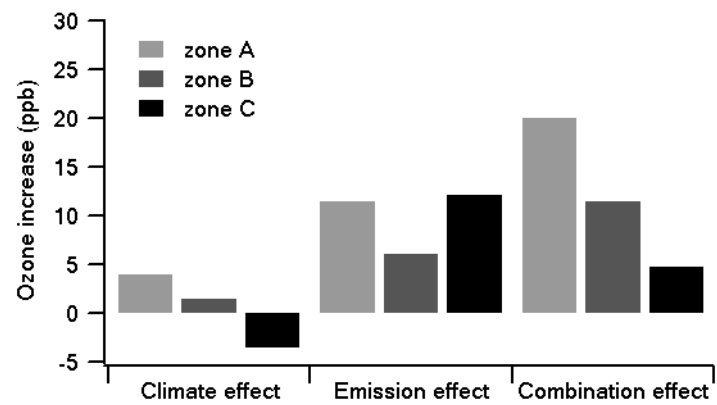


Figure 11. Changes in afternoon average surface O₃ concentrations induced by climate change, anthropogenic emission change, and combined change from the 2000s to the 2050s in three different regions.

Table 1 The grid settings, physics and chemistry options used in this study

Items	Contents
Dimensions(x, y)	100, 100/82,79
Grid size (km)	45/15
Vertical layers	28
Time step (s)	180
Microphysics	WRF Single-Moment 6-class scheme(Hong and Lim, 2006)
Long wave Radiation	RRTM scheme (Mlawer et al., 1997)
Shortwave Radiation	Goddard shortwave (Chou and Suarez, 1994)
Surface Layer	Moni-Obukhov scheme ((Monin and. Obukhov, 1954)
Land Surface	Noah Land-Surface Model (Chen and Dudhia, 2001)
Planetary Boundary layer	YSU scheme (Hong and Pan, 1996)
Cumulus Parameterization	Kain-Fritsch scheme (Kain, 2004)
Chemical Mechanism	CBMZ (Zaveri and Peter, 1999)
Photolysis scheme	Fast-J photolysis (Wild et al., 2000;Barnard et al., 2004)
Aerosol Module	MOSAIC using 8 sectional aerosol bins (Zaveri et al., 2008)

Table 2. Five cases of numerical experiments conducted in this study

Simulation	Period	Description
CL2000EM2000	October 2005-2007	2000s CCSM3 meteorological fields and biogenic emissions; INTEX-B anthropogenic emissions;
CL2050EM2000	October 2055-2057	2050s CCSM3 meteorological fields and biogenic emissions; INTEX-B anthropogenic emissions;
CL2000EM2050	October 2005-2007	2000s CCSM3 meteorological fields and biogenic emissions; future anthropogenic emissions;
CL2050EM2050	October 2055-2057	2050s CCSM3 meteorological fields and biogenic emissions; future anthropogenic emissions;
METH2050	October 2056	2056 CCSM3 meteorological fields and biogenic emissions; INTEX-B anthropogenic emissions;2050s CH4 concentration;

Table 3. Monthly average O₃ concentrations at 10 sites over PRD region during the October of 2006 and 2007

	LH	WQS	TH	LY	SD	HJ	DH	XP	HG	ZML	Mean
Obs	24.73	38.27	47.37	28.00	34.30	31.03	31.97	41.30	30.10	38.97	34.60
Sim	30.77	33.40	43.24	29.12	31.64	29.16	30.81	39.47	37.85	31.90	33.74